Journal of *Marine Science and Engineering*

MDPI

*Article*

# The Tsunami Caused by the 30 October 2020 Samos (Aegean Sea) $M_w$7.0 Earthquake: Hydrodynamic Features, Source Properties and Impact Assessment from Post-Event Field Survey and Video Records?

**Ioanna Triantafyllou [1,*], Marilia Gogou [1], Spyridon Mavroulis [1], Efthymios Lekkas [1], Gerassimos A. Papadopoulos [2] and Manolis Thravalos [3]**

[1] Department of Geology & Geoenvironment, National & Kapodistrian University of Athens, 15784 Athens, Greece; mgogou@geol.uoa.gr (M.G.); smavroulis@geol.uoa.gr (S.M.); elekkas@geol.uoa.gr (E.L.)
[2] International Society for the Prevention & Mitigation of Natural Hazards, 10681 Athens, Greece; gerassimospapadopoulos2@gmail.com
[3] Studio Reeldrone, Ippokratus 6, 83100 Vathy, Samos, Greece; meteographer@gmail.com
* Correspondence: itriantaf@geol.uoa.gr

**Abstract:** The tsunami generated by the offshore Samos Island earthquake ($M_w$ = 7.0, 30 October 2020) is the largest in the Aegean Sea since 1956 CE. Our study was based on field surveys, video records, eyewitness accounts and far-field mareograms. Sea recession was the leading motion in most sites implying wave generation from seismic dislocation. At an epicentral distance of ~12 km (site K4, north Samos), sea recession, followed by extreme wave height (h~3.35 m), occurred 2′ and 4′ after the earthquake, respectively. In K4, the main wave moved obliquely to the coast. These features may reflect coupling of the broadside tsunami with landslide generated tsunami at offshore K4. The generation of an on-shelf edge-wave might be an alternative. A few kilometers from K4, a wave height of ~1 m was measured in several sites, except Vathy bay (east, h = 2 m) and Karlovasi port (west, h = 1.80 m) where the wave amplified. In Vathy bay, two inundations arrived with a time difference of ~19′, the second being the strongest. In Karlovasi, one inundation occurred. In both towns and in western Turkey, material damage was caused in sites with h > 1 m. In other islands, h ≤ 1 m was reported. The h > 0.5 m values follow power-law decay away from the source. We calculated a tsunami magnitude of $M_t$~7.0, a tsunami source area of 1960 km$^2$ and a displacement amplitude of ~1 m in the tsunami source. A co-seismic 15–25 cm coastal uplift of Samos decreased the tsunami run-up. The early warning message perhaps contributed to decrease the tsunami impact.

**Keywords:** Samos 2020 tsunami; post-tsunami survey; wave run-up; tsunami velocity; tsunami magnitude; tsunami source area; tsunami impact; early warning; tsunami hazard assessment



**Citation:** Triantafyllou, I.; Gogou, M.; Mavroulis, S.; Lekkas, E.; Papadopoulos, G.A.; Thravalos, M. The Tsunami Caused by the 30 October 2020 Samos (Aegean Sea) $M_w$7.0 Earthquake: Hydrodynamic Features, Source Properties and Impact Assessment from Post-Event Field Survey and Video Records?. *J. Mar. Sci. Eng.* **2021**, *9*, 68. https://doi.org/10.3390/jmse9010068

Received: 9 December 2020
Accepted: 4 January 2021
Published: 11 January 2021



## 1. Introduction

On 30 October 2020, 11:51:27 UTC, a large shallow earthquake of moment magnitude $M_w$ = 7.0 ruptured the eastern Aegean Sea area to the north of the island of Samos, Greece, and caused a powerful tsunami (Figure 1) [1–3]. The earthquake focal parameters are summarized in Table 1. Consistent focal mechanisms produced by several seismological institutes showed E–W normal faulting (Figure 1) with the fault plane very likely dipping towards north [3,4]. These geometric features of the fault plane are consistent with the seismotectonic setting of the area [5–8]. In Samos, the most important earthquake impact included two fatalities, 19 minor injuries and damage to hundreds of houses, churches and port infrastructures. In the area of west Turkey, however, at least 114 people are known to have died due to the collapse of buildings and more than 1030 were injured.

Tsunami inundation was reported from Samos and other Greek islands as well as from several coastal sites of western Turkey. Remarkable material damage was caused by the tsunami. In the coast of western Turkey, one fatality was reported [2]. The 2020 Samos tsunami has been recorded by tide-gauges only in the far-field domain at epicentral distances larger than 110 km (Figure 1) due to the lack of stations in the near-field domain. However, these records proved extremely useful to calculate the tsunami magnitude, $M_t$, and to continue an effort, that started in recent years, for the creation of a tsunami magnitude scale in the Mediterranean Sea.

In Greece, the General Secretary for Civil Protection disseminated to residents of the eastern Aegean Sea Greek islands a tsunami warning sms via the European emergency phone number 112. The warning message was sent at 14:15 local time (12:15 UTC).

Other important earthquake associated phenomena, such as co-seismic coastal uplift and several types of ground failures, e.g., landslides, soil liquefaction, ground fissures and others, were also reported from Samos [1,3]. The co-seismic coastal uplift observed in Samos is of particular interest for the evaluation of the tsunami inundation and run-up in this island.

**Table 1.** Focal parameters of the Samos 30 October 2020 earthquake. For institute information, see Appendix A; h is focal depth, $M_w$ is moment magnitude. Earthquake origin time is 11:51:24 (NOA).

| Institute | Epicenter (N°/E°) | h (km) | Mw |
|---|---|---|---|
| GCMT | 37.76/26.68 | 12 | 7.0 |
| NOA | 37.9001/26.8057 | 6 | 6.9 |
| EMSC | 37.91/26.84 | 10 | 7.0 |
| GFZ | 37.90/26.82 | 10 | 7.0 |
| USGS | 37.918/26.790 | 21 | 7.0 |

In the eastern Mediterranean region, large tsunamis are generated mainly by earthquakes occurring in association with the lithospheric subduction process along the Hellenic trench (Figure 1) [9,10]. Large tsunamis have also been historically generated from volcanic eruptions in the south Aegean Sea, particularly in the Thera (Santorini) island complex (Figure 1). In the eastern Aegean Sea, however, although long seismic history has been historically reported [11], the tsunami record in the area is poor [9,10]. In the 20th century, the largest earthquakes in the area of Samos occurred on 11 August 1904 and on 16 July 1955 [12] (Figure 1). The moment magnitude of the 1904 event was $M_w$ = 6.8 [12] or $M_w$ = 6.0 [13]. For the 1955 event, $M_w$ = 6.9 [12], 6.7 [13] and 6.57 [14] was calculated. A tsunami of ~2 m in height that inundated ~20 m inland in Pythagorion, south coast, was reported in association with the earthquake of 1955 [12]. The very strong tsunami, generated by the distant large earthquake ($M_w$ = 7.7, [14]) of 9 July 1956 in the south Aegean Sea (Figure 1), was reported [15,16] to inundate the south coast of Samos but also the Vathy town at the north coast.

In this paper, we study the hydrodynamic features as well as the impact of the 30 October 2020 tsunami as observed in several sites along the coasts of Samos and of other Aegean Sea Greek islands. Post-event field survey data collected in the western Turkey coast [2] have also been utilized. In addition, we investigate the tsunami wave height decay away from the source, the dimension of the tsunami source area and the tsunami magnitude by utilizing wave heights measured in mareograms recorded in the far-field domain as well as heights observed in the field.

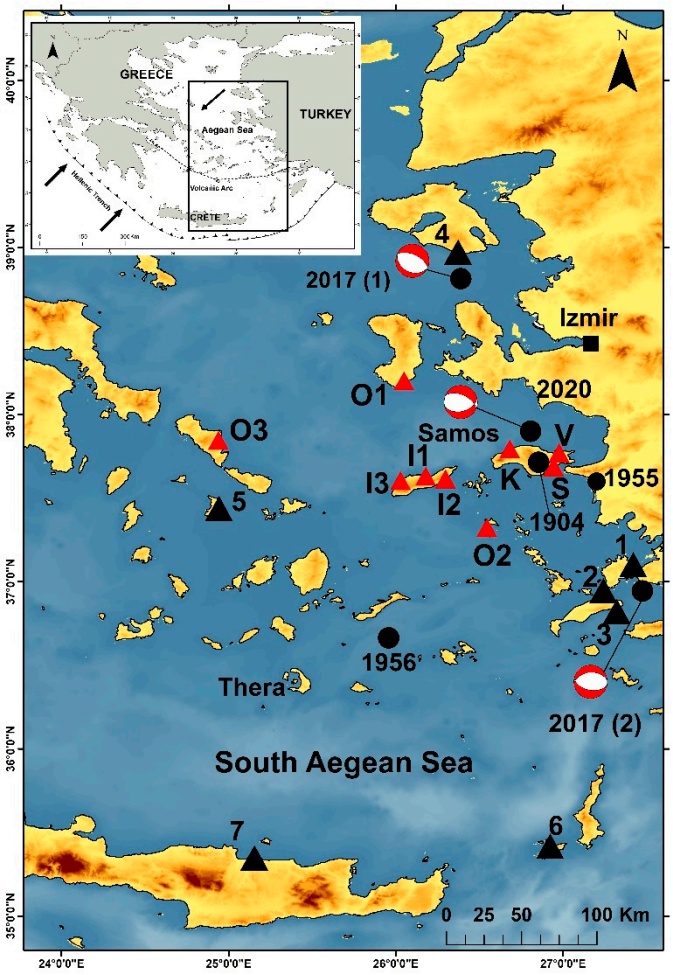


**Figure 1.** Map showing the record of the tsunami generated by the Samos earthquake on 30 October 2020: black triangle shows tide-gauge station, 1 = Bodrum, 2 = Kos, 3 = Kos-Marina, 4 = Plomari, 5 = Syros, 6 = Kasos, 7 = Heraklion; red triangle shows main sites of tsunami observation: Samos Isl., V = Vathy, K = Karlovasi, S = south Samos; Ikaria Isl.: I1 = Evdilos, I2 = Ayios Kirykos, I3 = Gialiskari; O1 = Komi (Chios Isl.), O2 = Scala (Patmos Isl.), O3 = Nimporio (Andros Isl.) (for more details, see in text); black circles show epicenters of earthquakes mentioned in the text, 2017 (1) and 2017 (2) stand for the 12 June and 20 July earthquakes, respectively; beach-ball shows earthquake focal mechanism, from moment tensor solution, indicating E–W normal faulting (from National Observatory of Athens, https://bbnet.gein.noa.gr/HL/seismicity/mts/revised-moment-tensors). Arrow in inset shows direction of lithospheric plate motion. Along the Hellenic trench, active lithospheric subduction and roll-back takes place, while the Aegean Sea area is dominated by back-arc normal faulting.

## 2. Materials and Methods

### *2.1. Methods Outline*

To study the Samos 2020 tsunami, we analyzed data sets compiled from various data sources, which included: (1) post-event field surveys, (2) tide-gauge records, (3) a series of video records from security cameras and mobile phones, (4) contacts with local authorities, and (5) eyewitness accounts and photos. In Samos, an initial post-event field survey was conducted by our team from the 31st October up to the 2nd November 2020. Additional surveys in selected sites were performed by team members in various dates until the 28th November 2020. In other islands, field observations, pictures and video records were collected by local collaborators of our team, namely by the civil protection officer in Chios island and by a tectonic geologist in Andros island, respectively (see Acknowledgments section). Observations from the islands of Ikaria and Patmos were

collected after communications with local port authorities and eyewitnesses who provided information and video records.

During our field-trips, we measured wave run-up, h (in m) above the sea level (asl) unless otherwise indicated, and inundation intrusion (run-in), d (in m), from the shore. Our measurements were based on water markers left in walls, in other objects or in the ground. Schematic explanations of the terminology used can be found in Figure 2. In contucting post-tsunami surveys, we followed relevant guidelines [17,18]). Values of h and d have also been estimated from the analysis of video records and the evaluation of eyewitness accounts. All times reported are in UTC unless otherwise indicated. Reference earthquake epicenter is the one determined by NOA (Table 1).

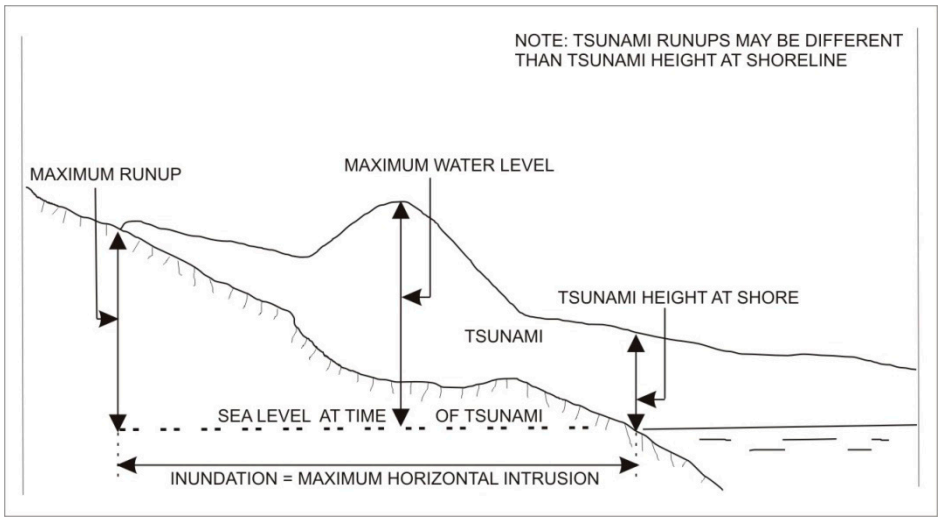


**Figure 2.** Schematic explanation of some commonly used tsunami terms (adapted from [18] as modified from [9]; similar terms have been adopted in the Intergovernmental Oceanographic Commission IOC Tsunami Glossary 2019, http://itic.ioc-unesco.org/index.php?option=com_content&view=article&id=2078&Itemid=2306; last access November 2020). The term "run-in" may be used instead of inundation. The term "tsunami amplitude" is in use by some authors to describe either tsunami height at sea shore or wave amplitude in the open sea. The term "flow depth" is also used instead of "run-up" for the tsunami height above the ground, at a specific location, as indicated by water markers.

In Samos, field observations were performed in a long number of coastal points grouped in 18 sites (Figure 3). In the north coast, which was the most severely hit by the tsunami, 14 sites were investigated. Four sites were also examined in the south coast. Tsunami observations were also collected from 6 sites in other islands: Ikaria (3 sites), Chios, Patmos and Andros islands (Figure 1). Minor tsunami inundation was also reported from other islands, including Fourni and Mykonos, but no specific information has been collected. In some observation sites, two main inundations occurred within a time difference of only ~20 min. However, no tide-gauge records of the tsunami are available in the near-field domain and this does not help, neither to determine features of the leading wave nor to distinguish clearly the features of the first inundation from those of the second one. Nevertheless, our research in this respect has been successfully supported from video records analysis combined with eyewitness accounts in several observation sites. Observations included in an early report regarding tsunami features observed in selected coastal segments of western Turkey [2] have also been taken into account.

From the observations collected, we evaluated the tsunami impact and measured wave hydrodynamic parameters including the number, modes and times of wave arrivals, as well as run-up and run-in values. For some occasions, we have been able to calculate the wave velocity offshore as well as the upstream water velocity utilizing accurate arrival times from video records. It has not been possible, however, to calculate all parameters

in all the observation sites due to a lack of appropriate data. For the tsunami magnitude calculation in $M_t/M_w$ scale, we utilized wave height recorded in far-field mareograms. Wave run-up values found in near- and mid-field distances, in both the Greek islands and western Turkey, have been considered as proxy wave heights, which were tested also to calculate $M_t$ and to approach the decay of the tsunami wave height with the increase in distance from the source. In addition, from empirical global relationships for tsunamigenic earthquakes, we estimated the area of the tsunami source and the displacement amplitude at the source.

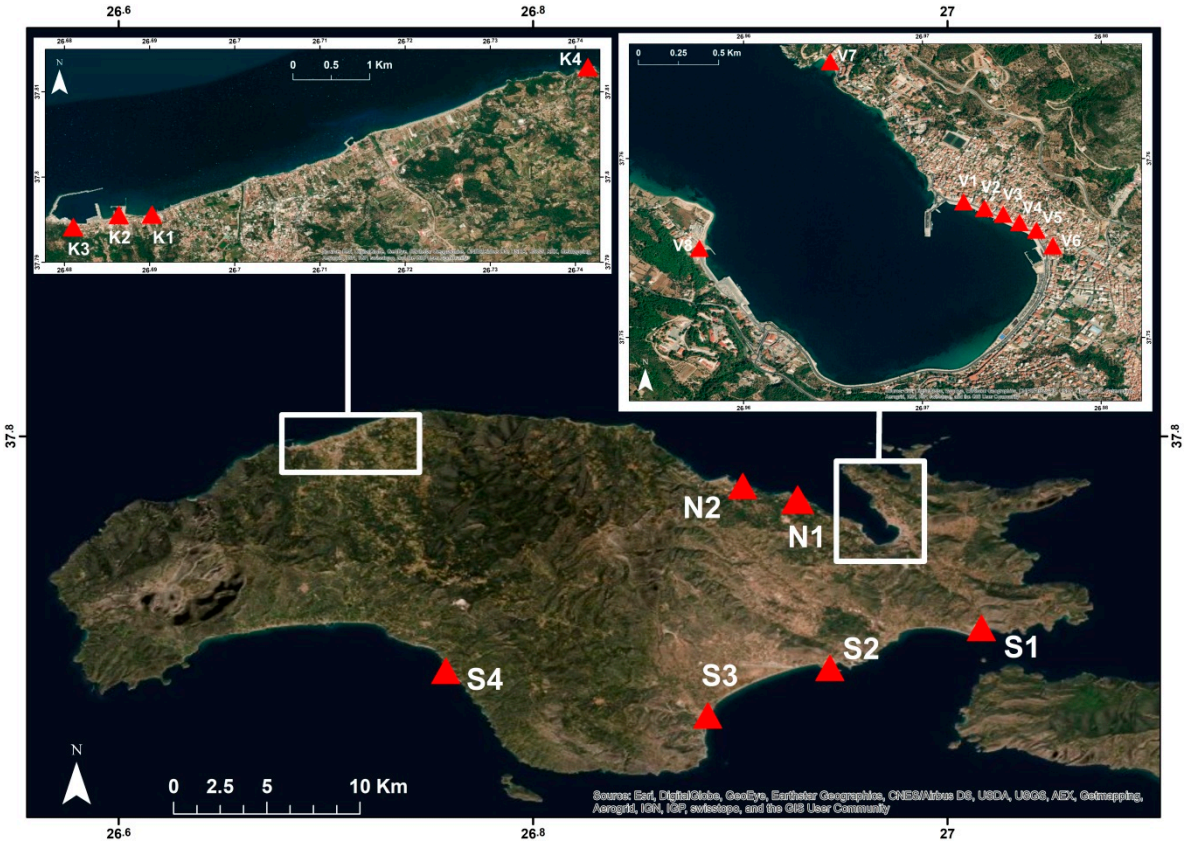


**Figure 3.** Sites of tsunami field-survey in Samos: V1–V6 = Vathy town, V7 = Gagou beach, V8 = Malagari, N1 = Kedros, N2 = Kokkari, K1–K3 = observation sites in Karlovasi town, K4 = Ayios Nikolaos; S stands for south Samos coasts, S1 = Psili Ammos, S2 = Pythagorion Port, S3 = Heraion, S4 = Kampos. For more details, see the text.

### 2.2. Tsunami Observations

In the next subsections, we describe the observations collected and the tsunami hydrodynamic parameters measured. We also evaluate the tsunami impact in each one of the 24 coastal observation sites examined in Samos and other islands in the Aegean Sea. Each observation site is codified by a respective code number, the site name, the site distance D from the shore, when relevant, and the geographical coordinates in degrees.

#### 2.2.1. Samos Island

There are two main observation areas in Samos, the Vathy and Karlovasi towns (Figure 3), with populations of 8079 and 6708, respectively, according to the 2011 national census. In Vathy, which is the main town of the island, the residential and tourist zone exposed to the tsunami attack is situated along the eastern side of the bay. From the urban planning point of view, the coastal zone in Vathy town consists of three parallel lanes, which from the shore towards inland are: a pedestrian lane, the two-way main road and a second pedestrian lane (Figure 4). Along the inland pedestrian lane one may find various

hotels, banks, shops, offices, cafes, restaurants and other commercial stores. Narrow streets perpendicular to the main road drive further inland. At the northwest, the coastal zone is "protected" by the port. In Vathy coastal zone, the ground level of the seawards pedestrian lane was measured at ~0.6 m asl. The western side of the bay is not a residential and tourist zone but is dominated by the new commercial port, a small marina and a free beach. In the area of Vathy bay, from the 8 sites examined, six are situated in the southeast coast of the bay along the town coastal zone (V1–V6), one in the northeast bay coast (V7) and another in the southwest bay coast (V8) (Figure 3).

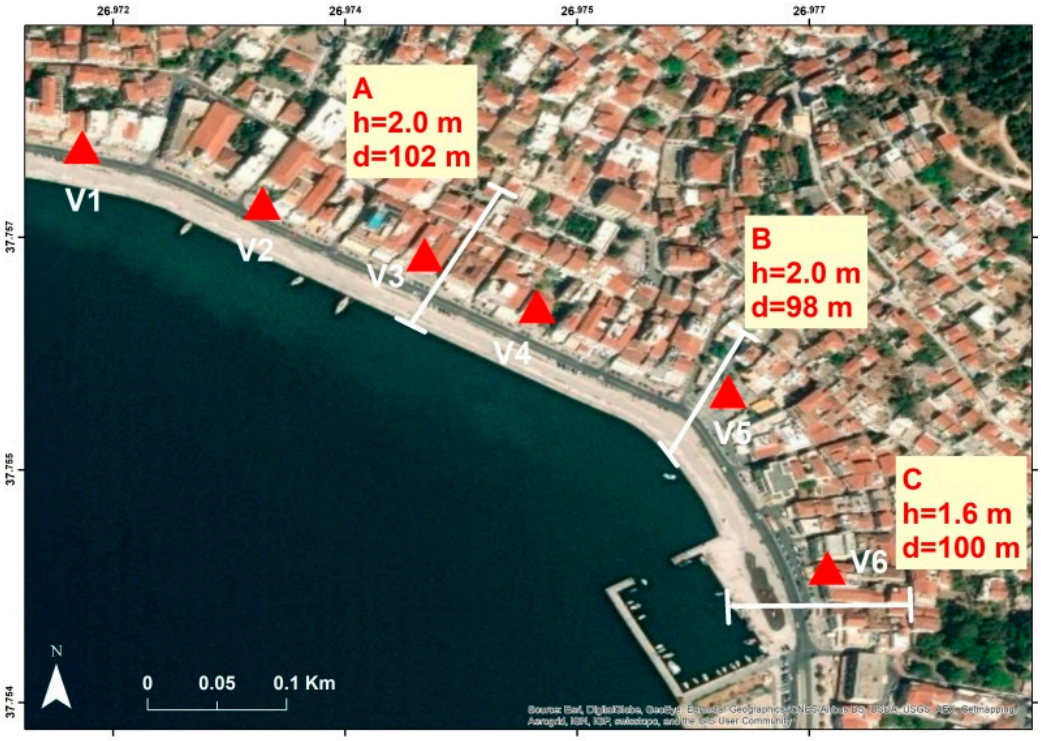


**Figure 4.** Observation sites V1 to V6 (red triangles) along the Vathy bay east coast and three characteristic tsunami transects A, B, C (white lines), measuring maximum run-up, h, at respective run-in distance, d (for details, see in text).

In Karlovasi town, the urban planning features are similar to those in Vathy. Three observation sites (K1–K3, Figure 3) of main interest are situated in the area of the port and of the nearby marina. The ground level of the coastal pedestrian zone in front of the Port Authority building was measured at ~1.1 m asl. Another site of great interest is the Ayios Nikolaos beach (K4) situated ~5.8 km east of Karlovasi. In between Ayios Nikolaos and Vathy town, two sites were examined in Kedros (N1) and Kokkari (N2) (Figure 3). In the south coast, the four sites examined are shown in Figure 3.

Samos North Coast

In Vathy town, apart from the detailed description of our findings in each observation site examined, three representative run-up transects are also highlighted (Figure 4).

*V1. Hertz office (D~35 m, 37.757584, 26.972299).* Two video records from one external and one internal security camera, showing strong tsunami inundation along the coastal zone, were provided by the office owner. The time in both video records was found delayed by 3 min and 18 s in relation to the video recorded by another security camera at site V4, which accurately recorded the earthquake at 11:51:34. The corrected time is hereafter used for the videos in site V1. The video from the external security camera starts at 12:22:46, showing that the area was already wet, apparently due to the first inundation. At that time, a second tsunami inundation just started and gradually inundated the entire distance of

35 m from the shore. The video shows people running to evacuate (Figure 5a), cars floating and fishes swimming towards the sea (Figure 5b). From the field inspection and the video analysis, we estimated a run-up of h = 1.4 m asl at run-in distance d~35 m. The upstream water velocity was estimated at 1.4 m/s. Unfortunately, no video record has been available for the first inundation and, therefore, we roughly estimated d~30 m and h~0.85 m asl.


(**a**) (**b**)

**Figure 5.** Site V1. Inundation starts at 12:22:46, people run to evacuate (**a**). At ~12:26, general flooding is noticed, cars float (**b**) (video time is corrected, see details in text; photo credit, Hertz office).

The video from the interior camera starts at 12:23:54. Outside of the office entrance door, the water level was already at h~0.6–0.7 m from the ground level. A few seconds later, the water opened the door violently and flowed into the office, causing material damage. In interior walls, we measured water marks at h~0.4 m from the office floor. Then, for the second wave inundation in site V1, we estimated h~1.6 m asl at d~40 m from the shore.

*V2. Zen fish restaurant (D~35 m, 37.757222, 26.973464).* The second wave hit the restaurant violently, causing remarkable material damage (Figure 6a). Water marks of sand traces and small seaweed pieces were left on walls in the small street perpendicular to the main coastal road at d = 45 m from the shore. We measured a run-up of h = 1.09 m from the ground level (Figure 6b) or h = 1.69 m asl.

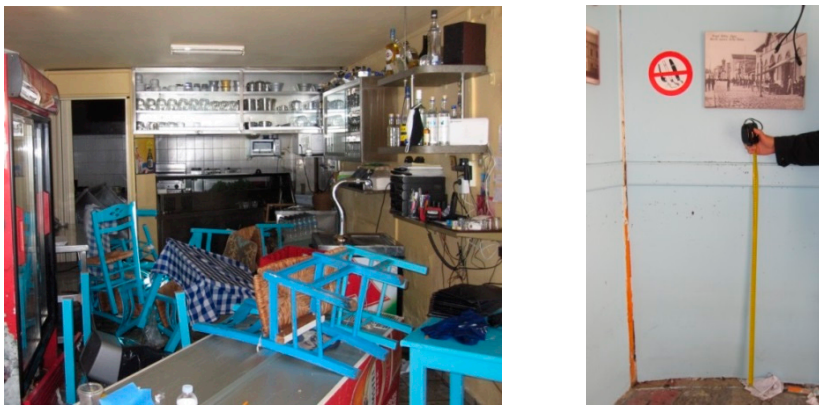

(**a**) (**b**)

**Figure 6.** Site V2. Indoor material damage caused by the tsunami attack in the fish restaurant (**a**). Water mark at h~1.09 m was measured at a run-in distance of 45 m (**b**) (photo credit, I. Triantafyllou).

*V3. Piraeus Bank (D~35 m, 37.756724, 26.974580).* The second wave inundated the entire coastal zone and through a network of small streets, either perpendicular or parallel to the main coastal road, inundated at run-in distances of up to d = 102 m. Material damage was caused in several shops. The area was extensively littered while sand and pebbles were left behind. From water marks left on walls (Figure 7) along the transect 1 (Figure 4), we measured a run-up of h = 1.7 m asl at d = 95 m. Eventually, we measured a maximum run-up of h = 2.0 m asl at d = 102 m.

(**a**) (**b**)

**Figure 7.** Site V3. In Xrisostomou Smirnis street, close to the "Garden Restaurant", we measured h = 0.3 m (**a**) and h = 0.24 m (**b**) above ground level at d = 85 m and 87 m, respectively. The value of h minimized at d~102 m, where we estimated maximum h = 2.0 m asl (photos credit, I. Triantafyllou).

*V4. Library (D~35 m, 37.756457, 26.975358).* A valuable video record of both inundations has been obtained from an external security camera. The video timer was absolutely accurate, as one may conclude from the record of the earth shaking at 11:51:34. The video time in site V4 has been used as reference for the correction of time in the site V1 videos. The first tsunami inundation on the seawards pedestrian zone, i.e., at a height of 0.6 m asl, was recorded at 12:04:15. People are seen running to escape (Figure 8a). The inundation covered the entire zone of 35 m (Figure 8b) and flowed upstream in a nearby small street. Water retreat started at ~12:06.

(**a**) (**b**)

**Figure 8.** Site V4. First tsunami inundation starts at 12:04:15, people run to escape (**a**). In less than 1 min the coastal zone inundated, car drivers try to go back (**b**) (photos credit, Samos Library).

The second and strongest inundation arrived at 12:24:10 (Figure 9a,b). From the video record and the field inspection in front of the building, at run-in distance d = 35 m from the shore, we estimated run-ups of h~1.15 m asl and h~1.4 m asl for the first and second tsunami waves, respectively. The second wave penetrated further inland through the nearby small street which, however, is not shown in the video record. No water marks were found there and, therefore, no estimation of the final run-in and run-up has been made for this observation site. In the coastal zone, the upstream water velocity, v, was calculated as $v_1$ = 0.8 m/s and $v_2$ = 0.92 m/s for the first and second tsunami wave, respectively. The wave velocity in the bay from site V1 to site V4 (distance 280 m) was found to be as low as 3.3 m/s (or 12 km/h). Water retreat after the second inundation started at about 12:27. Cars were left behind at levels higher than the road level (Figure 10a). At around 12:30, the sea level at the bay head dropped by ~0.7 m below its normal position (Figure 10b), i.e., ~1.3 m below the pedestrian zone level.

(a) (b)

**Figure 9.** Site V4. Second tsunami inundation starts at 12:24:10 (**a**). In less than 1 min all the coastal zone flooded; the book stand was drifted away and after a few seconds it disappeared (**b**) (photos credit, Samos Library).

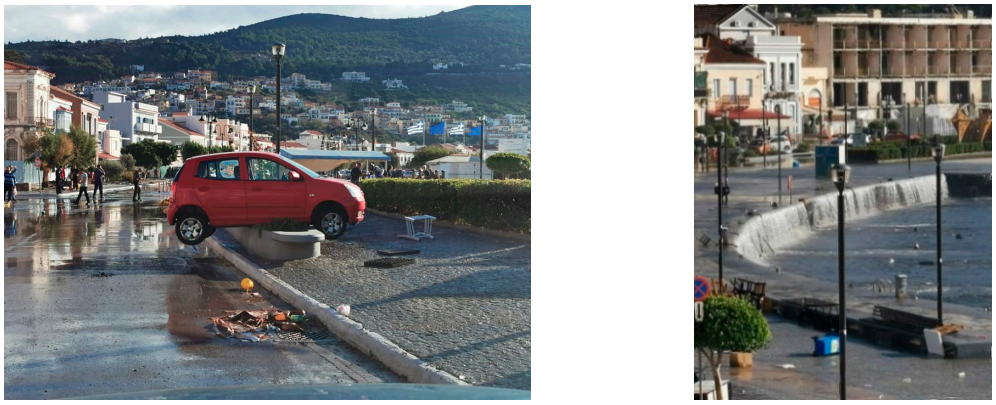

(a) (b)

**Figure 10.** Sites V4–V5, after the second inundation: characteristic picture of what was left behind (**a**); sea level drop by ~0.7 m below its usual position during water retreat (**b**) (photos credit, Manolis Pyrgiotis).

*V5. Pythagoras or Lion Square (37.755993, 26.976371).* In this locality, the two inundation phases have been documented in several video records (Figures 11 and 12). The owner of a kiosk at d~31 m (Figure 11a) estimated h~1 m above the street level. We found no water marks there but from eyewitness accounts and several publically available videos we were able to verify the run-up reported in the kiosk area. Then, we obtained h~1.6 m asl. Further inland, at d~75 m, the water entered a Pharmacy (Figure 11b). From the Pharmacy's owner account and the wet traces found on walls, we estimated h~0.3 m above the ground level just in front of the Pharmacy's entrance. The water flowed further upstream (Figure 12a) and inundated for another ~23 m inland (Figure 12b). After talking with eyewitnesses and from a video record analysis (Figure 12b), we concluded that the maximum run-up at the upper side of the square (d = 98 m, transect 2, Figure 4) reached h~2.0 m asl.


(a) (b)

**Figure 11.** Site V5. After the first tsunami inundation, the entire square is still wet. The second tsunami arrival already starts (**a**), people watch towards the sea side (**b**). Arrows in (**a**) and (**b**) show the kiosk and the Pharmacy mentioned in text (photos credit, Samos.24).


(a) (b)

**Figure 12.** Site V5. Water flow upstream (arrow) during the second inundation (**a**). At the upper square side (d = 98 m), the water depth reached only a few cm (**b**). Run-up h~2 m asl has been estimated. Most people evacuated but a few look like enjoying the inundation (photos credit, Samos.24).

*V6. Zarbanis commercial gallery (D~85m, 37.755382, 26.977227).* In a commercial gallery, perpendicular to the main road, a video record from security camera shows pedestrians and motorcyclists running to escape the second wave inundation (Figure 13a). From the video and the field inspection, we estimated a maximum h~1.6 m asl at the point of the advertisement stand shown in Figure 13b, at d~100 m. The upstream water velocity was estimated to be equal to ~1 m/s. Along the coastal zone, fishes and extensive littering were left behind by the wave.

(a) (b)

**Figure 13.** Site V6. People realize that inundation starts and run inland to evacuate (**a**). In less than one minute, the gallery was inundated (**b**) (photos credit, SamosToday.gr).

*V7. Gagou beach, northeast Vathy bay (37.765419, 26.964838).* In this beach (Figures 3 and 14), a local resident was sunbathing when the ground shook. According to the eyewitness, the leading tsunami wave phase arrived ~10 min after the earthquake and inundated up to d~4–5 m. The second tsunami wave was noted about 15 min after the

first and penetrated inland up to d~6–7 m. The eyewitness reported that the maximum inundation line was determined by the seaweed line left behind in the beach (Figure 14). The estimated maximum run-up did not exceed h~0.4 m. The eyewitness said that after the second inundation the sea oscillated another 2–3 times with periods of about 10–15 min.

**Figure 14.** Site V7. Tsunami water mark was found at ~6–7 m from the shoreline. The eyewitness is shown sunbathing in front of the white wall (photo credit, I. Triantafyllou).

*V8. Malagari beach, southwest Vathy bay (D = 17 m, 37.754984, 26.957526).* The owner of a local cantina (Figures 15 and 16a), who experienced the tsunami himself, reported material damage due to run-up of h~1.1 m. In a fence wall at ~3 m further inland, we measured h = 1.25 m asl. The eyewitness said that from the three small fishing boats he had onshore nearby the cantina, only one remained standing. One boat was lost in the sea, while another one was dragged by the wave and left in a new position ~20 m away (Figures 15 and 16a). Ground erosion was locally caused during the wave withdrawal process (Figure 16b). The beach and the nearby pier were found covered by sea sand and salt. In the same area, an iron container of 13 m × 2 m × 2 m in dimension was drifted away for about 8–9 m and rotated ~35° counterclockwise (Figures 15, 16a and 17). According to Port Authority officers, the container was full of marine anti-pollution equipment. We roughly estimated the container weight at ~10 t.


**Figure 15.** Site V8. Tsunami run-up of h~1.25 m was measured at d = 20 m (yellow arrow). A boat was drifted away by ~20 m (blue arrow, see also Figure 16). Another boat was lost in the sea (orange arrow). An iron container (red arrow, pre-seismic position) was moved away by ~8–9 m and rotated ~35° counterclockwise (see also Figures 16a and 17).

(**a**) (**b**)

**Figure 16.** Site V8. Run-up of h~1.25 m was measured behind the local cantina (yellow arrow) (**a**). The tsunami moved a boat ~20 m from its initial position (blue arrow). The iron container moved by the tsunami is seen on the left hand side. The coast near the new boat position was eroded during the tsunami withdrawal (orange arrow) (**b**) (photos credit, I. Triantafyllou).

**Figure 17.** Site V8. The tsunami moved an iron container, from its initial position on the pier, by ~8–9 m (arrow). In the background, the Vathy town is seen (photo credit, I. Triantafyllou).

*N1. Kedros beach (37.771112, 26.926588).* A local resident, a forester by education and specializing in the management of the natural environment, reported that he observed water oscillations starting with a sea recession of ~3–5 m within ~20 min from the time of the earthquake. The main sea level rise occurred ~25 min after the earthquake with run-up ~0.8 m at inundation distance of ~5 m.

*N2. Kokkari beach (37.778453, 26.897073).* A local resident reported that ~10 min after the earthquake she observed sea level rise of ~1.0 m and water whirlpools (Figure 18). She has not been confident, however, if sea recession was the first motion or not.

**Figure 18.** Site N2. According to a local resident, the tsunami moved as shown by the arrow, i.e., from NW to SE; the sea level rise completely covered the short "neck" connecting the land with the islet (photo credit, Ioanna Georgoudi).

*K1. East of marina (D~5 m, 37.7954227, 26.6884454).* Two videos taken at this site of Karlovasi (Figure 19) with a mobile phone camera showed a sea recession for several meters soon after the earthquake. This is consistent with observations collected at sites K3 and K4.


**Figure 19.** Sites of field observations in the Karlovasi vessels shelter (marina, circle) situated to the east of the port. Yellow arrow shows site K1. A–F are observation points in site K2. Double red arrow shows an inundation transect adjacent to the port authority building, K3.

*K2. Marina area (37.795559, 26.6869867).* This observation site is of complex coastal configuration due to the presence of beaches to the west and east of it and of a long break wall to the northwest. This complexity did not allow us to reliably measure the wave run-up. However, we were able to determine the inundation line from water marks found in the localities A, B and C (Figures 19–21). In locality B, the wave penetrated inland, overtopped the narrow pedestrian zone and reached the main road at d~84 m from shore. In localities A and C we measured d = 75 and d = 65 m, respectively. Light wooden structures were moved from their initial positions (localities D and E, Figure 21a,b) while a small boat was moved ashore on a pier at h~0.7 m (locality F, Figure 22a). This is a minimum wave height in the site K2. Between the localities C and D, the goal posts of a small football terrain were displaced, while the perimeter fences were deformed by the tsunami inundation and retreat.

(**a**) (**b**)

**Figure 20.** Site K2. Water marks in positions B (**a**) and C (**b**) shown in Figure 19 (photos credit, M. Gogou).

(a) (b)

**Figure 21.** Site K2. In position D (Figure 19), a wooden structure of the cultural association of Karlovasi was dragged away from its initial position for ~10 m (**a**); in position E (Figure 19), a similar structure was displaced upwards (**b**) (photos credit, M. Gogou).

(a) (b)

**Figure 22.** In position F (site K2, Figure 19), the wave overtopped the pier (h~0.7 m) and moved a small boat ashore (**a**) (photo credit, M. Gogou). The Karlovasi pedestrian zone in front of the Port Authority building (K3, Figure 19) inundated ~8 min after the earthquake (**b**) (photo credit, video by Port Authority).

*K3. Port Authority building (D = 35 m, 37.7942081, 26.6805076).* A fisherman reported that being onboard near the Karlovasi Port he felt the earthquake violently. He also observed a sea level drop exceeding ~1 m in amplitude and water recession of more than 15 m. Boats were stranded as if on dry land. This was verified from an independent local resident being at the seashore during the event. A few minutes later, inundation followed and the water covered the coastal pedestrian zone.

The eyewitness accounts are verified by a video record available to the Port Authority showing sea level recession occurring soon after the earthquake on ~11:57:30. A couple of minutes later, inundation occurred (Figure 22b) and the water entered the Port Authority building but no damage was caused. The run-up was measured at 1.65 m asl. The local resident said that next to the Port Authority building, in a narrow street perpendicular to the shoreline and lying at lower level than the building, the water penetrated inland for another ~20 m (see transect position in Figure 19). Then, a maximum run-up of h~1.80 m asl was found at d~53 m. Sand and pebbles were left behind. Next to the small street, the wave violently entered a coffee-shop causing material damage.

From a video record shooting to the east of the Port Authority building, it is clear that the pedestrian zone was inundated violently by the wave, while people ran inland to escape. From the field inspection and the video records analyzed, we estimated run-up varying from h~1.60 m to h~1.70 m. Material damage was caused in stores. It is noteworthy that in Karlovasi only one inundation was reported.

*K4. Ayios Nikolaos beach (D~5.8 km east of Karlovasi Port, 37.8127922, 26.7414823).* This is a key site for two reasons: (1) it is the closest to the earthquake epicenter (Δ~12 km), (2) a video record, which comes from a security camera installed in a house situated in a settlement on steep slope very close to the shore (Figure 23a,b), provides a unique opportunity to accurately reproduce the timeline of the sea level changes. Field inspection and collection of eyewitness accounts completed our observation set. The house owner, an eyewitness of the event, reported that the camera is satellite synchronized and, therefore, the time is absolutely accurate. Before the earthquake occurrence, the level of the house entrance was situated at h~1.30 m asl. However, the house owner reported that with the earthquake the sea level in the area dropped by ~20 cm, which is consistent with our field survey indicating co-seismic coastal uplift in this site (Figure 23a), as well as in other coastal spots of the island [1,3]. The house entrance level beneath the camera was measured at 1.50 m asl (Figure 23b).


(**a**) (**b**)

**Figure 23.** Site K4. Team member performed measurements and found the house entrance level at a height of ~1.50 m asl, including the co-seismic uplift of ~20 cm (yellow arrow) (**a**). Heights asl in the door below the security camera (white arrow) are marked (**b**) (photos credit, M. Thravalos).

The video shows that on 11:53:33, i.e., nearly 2 min after the earthquake, a sea recession occurred (Figure 24a) at an estimated retreat distance of ~15 m and vertical draw-down ~1 m (Figure 24b). A small inundation occurred around 11:53:50 and the sea returned at its normal position. A new minor recession phase with a retreat distance of only ~5 m occurred around 11:55:00. Sea level rise followed once more (Figure 25a) and at 11:55:37 the tsunami reached its maximum height, inundated the house entrance (Figure 25b), opened the doors and swooped in the interior rooms (Figure 26a), causing material damage (Figure 26b). The highest water level was recorded at 11:55:42 (Figure 26a) and reached the external house wall at 3.50 m asl. Due to splash, however, the maximum wave height has been estimated at 2.80 m asl. The residents, who are seen in the video to evacuate only 30 s before the tsunami attack, reported that in the room the water reached 2.15 m above the room floor, which suggests a maximum water height of 3.65 m asl. This was concluded from seaweed pieces found on the water heater at the room top. However, considering again the splash effect, we estimated that the water level in the room may have reached ~3.35 asl.

(a) (b)

**Figure 24.** Site K4. Leading sea recession (arrow); footage from security camera shooting east (**a**), and footage of the sea recession taken from uphill eastwards of security camera (**b**) (photos credit: Cornilia Papakonstantinou, from security camera (**a**), and Athina Alexandrou, from mobile phone video (**b**)).

(a) (b)

**Figure 25.** Site K4. The wave propagated obliquely to the coast from east to west (arrow) (**a**) and inundated the entrance of the house (**b**) (photos credit, Cornilia Papakonstantinou from security camera).

(a) (b)

**Figure 26.** Site K4. The wave reaches maximum height (**a**); indoor material damage caused by the tsunami (**b**) (photos credit: Cornilia Papakonstantinou from security camera (**a**); Manolis Thravalos (**b**)).

Among all the sites examined, the shortest arrival times of both the leading wave and the largest wave height have been documented in site K4. The two wave phases arrived only 1 min and 43 s and 4 min and 25 s from the earthquake origin time, respectively. In the video record, it is clearly seen that the wave propagated alongside the beach from the east to the west. The distance from the east side of the small bay up to the house is ~125 m. We calculated a wave velocity of ~7.8 m/s or ~28 km/h along the beach. In the nearby cove, a few small boats were swept off. To roughly calculate the wave velocity in the offshore Karlovasi area, we considered that the time difference for the leading wave arrival from K4 to K3 was 4 min and 20 s, while the time difference of the first inundation arrival was

4 min and 10 s. Then, considering that the distance from K4 to K3 is ~5.8 km, we found a velocity of 23 m/s or 83 km/h.

The residents in site K4 reported that a second but smaller inundation arrived around 12:15. Unfortunately, it has not been recorded since the camera was out of order due to power outage. However, the second inundation did not move in parallel to the coast, as the first did, but it happened as a more or less uniform sea level rise along the shore. The water depth at the house entrance level due to the second inundation was estimated by the residents at ~10 cm, i.e., ~1.60 asl. The video recording came back soon showing a completely calm sea at ~12:31. Last, the residents recalled their parent's account that the area was also hit by the 9 July 1956 large tsunami (Figure 1).

Samos South Coast

*S1. Psili Ammos bay (37.7072114, 27.0166114).* In the sandy beach of the bay, we observed a wet zone of ~5–6 m in width as well as a line of seaweed situated at the same distance from the shoreline (Figure 27a). A local resident, an owner of sun beds and an eyewitness of the event, verified that the wet zone and the water mark were due to the tsunami inundation. He said also that the first wave arrived ~25–30 min after the earthquake. Possibly, this was the second wave observed in Vathy. After water retreat for ~20–25 m, the sea was slightly inundated again and oscillated 3–4 times with periods of ~10–15 min. We roughly estimated h < 0.5 m.

(**a**) (**b**)

**Figure 27.** Tsunami water marks in Psili Ammos beach, site S1 (**a**) and in Heraion beach, site S3 (**b**) (photos credit: G.A. Papadopoulos (**a**) and anonymous (**b**)).

*S2. Pythagorion town, port (37.6888896, 26.9433338).* Eyewitnesses from local restaurants said that the sea level oscillated 3–4 times with periods of ~10 min but no inundation was observed. We measured the mean height of the pier surface to range from ~0.6 m to ~0.7 m asl. The eyewitnesses were unable to specify the time and the mode of the first sea motion. We roughly estimated h < 0.5 m.

*S3. Heraion beach (37.6655967, 26.8846012).* A local resident that received the tsunami warning message ran to watch the wave and took the picture shown in Figure 27b. The picture shows a wet zone of 3–4 m in width, which indicates small tsunami inundation. Later we visited and verified the inundation line. We estimated h~0.4 m.

*S4. Kampos beach (37.7077302, 26.6975259).* A local resident, a civil engineer, reported that after the earthquake the sea level dropped by ~0.3 m and then rose by ~0.2–0.3 m above its initial position.

2.2.2. Ikaria Island

Observations were collected from sites: I1 and I2 at the north coast and I3 at the south coast (Figure 2).

*I1. Evdilos Port (37.6310116, 26.1768815).* Port Authority officers said that sea recession of ~5-10 m happened immediately after they had learned from their colleagues in Samos that the first wave had already arrived in Vathy town. This implies that in Evdilos the sea retreat occurred ~15 min after the earthquake. Then, inundation happened in the port and

the water covered one pier with its surface lying at ~0.7 m asl. This is verified by a video taken with a mobile phone camera (Figure 28a,b). The sea oscillation in the port repeated 2–3 times for about 1 h.

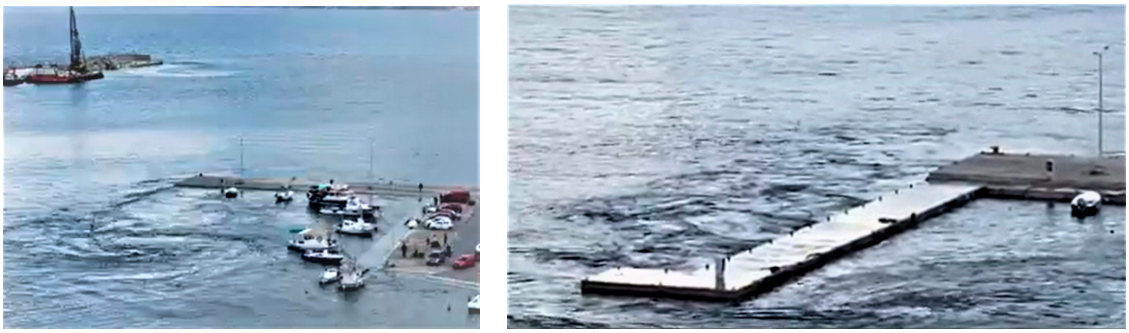

(**a**) (**b**)

**Figure 28.** Site I1, Ikaria island: footage during (**a**) and after (**b**) tsunami inundation (photos credit, Giannis Petrakis from mobile phone video).

*I2. Gialiskari marina (37.632358, 26.1032475).* An eyewitness reported that earthquake sea recession occurred first and was followed by inundation of ~2 m inland at a time of ~40 min after the earthquake.

*I3. Ayios Kirykos Port (37.6124802, 26.2935023).* Port Authority officers reported that sea recession of a few meters was observed about 20 min after the earthquake; sea level rise followed. The sea oscillation in the port repeated 2–3 times for about 1 h, as it did in Evdilos port, site I1. The waves did not inundate inland and no damage was reported. In a video taken from a security camera installed at considerable distance from the port, vessels are seen to leave the port and sail to open sea at ~12:10. One minute later, inundation occurred in the marina, which is situated closer to the camera. Therefore, we concluded that the first inundation in the port was noted at ~12:10. The same video shows a second sea level rise occurring in the marina at ~12:43. Both inundations reached the marina's pier level at h~1 m. The second inundation was likely stronger than the first one. After the first inundation, the sea was in continual oscillation until ~14:00.

#### 2.2.3. Other Islands

*O1. Komi village, Chios island (38.2036935, 26.0453001).* A local eyewitness reported to the civil protection officer of the island that, about ~1 h after the earthquake, sea recession by ~15 m was observed and ~3 min later tsunami run-up of h~1 m occurred in the nearby pier. In the beach, the run-in was estimated at 15–20 m. The sea oscillation continued for about 2–3 h. Four small vessels were crushed on the stone blocks of the breakwater (Figure 29). The vessels were moved by the tsunami from the nearby small marina of the village. The civil protection officer of the island reported that the tsunami was also noticed in the Emporios bay a few km to the south of Komi.


**Figure 29.** Site O1. Boats crushed on water break stones (photo credit, astraparis.gr).

*O2. Scala port, Patmos island (37.325107, 26.5429231).* From a video record taken with mobile phone camera, it comes out that part of the pier was inundated by the tsunami (Figure 30a,b); we roughly estimated h~0.4 m.

(**a**) (**b**)

**Figure 30.** Site O2. The pier during inundation (**a**) and after sea retreat (**b**) (photos credit, Patmostimes.gr).

*O3. Nimporio bay, Andros island, east coast (37.84470, 24.93581).* Dr. Nikos Mourtzas, tectonic geologist and collaborator of the survey team, was an eyewitness of the tsunami arriving at site O3 ~1 h after the earthquake. He provided footage from mobile phone video showing that the pier was slightly inundated. The eyewitness measured the pier level at h = 0.55 m asl.

Summary of Observations

The main tsunami observations collected in Samos and other islands are summarized in Table 2. Relevant data collected in localities of western Turkey [2] are listed in Table 3.

**Table 2.** Tsunami parameters measured or estimated (marked by ~) in observation sites of run-up > 0.5 m: Δ = epicentral distance, t = arrival time, h = run-up at run-in distance d, $h_{max}$ = maximum h value at $d_{max}$; signs (+) and (−) show sea level rise and drop, respectively; symbol ≥ means "at least"; dam = material damage (details in text).

| Observation Site | Δ (km) | t (UTC) | h (m) | d(m) | $h_{max}$(m) | $d_{max}$(m) | dam |
|---|---|---|---|---|---|---|---|
| SE Vathy, V4 (Samos Isl.)<br>SE Vathy, V1 to V6 (Samos Isl.) | 21.0<br>21.0 | 12:04:15 (+)<br>12:22:46(+)<br>12:30 (−) | 1.15 (+)<br>1.40 (+) | 35 (+)<br>35 (+) | 2.0 (+)<br>~0.7 (−) | 102 (+) | yes<br>yes |
| NW Vathy, V8 (Samos Isl.) | 21.0 | | | | 1.25 (+) | 20 (+) | yes |
| Kedros, N1 | 17.5 | ~12.11 (−)<br>~12.16 (+) | | | ~0.8 (+) | ~5 (−)<br>~5 (+) | no<br>no |
| Kokkari, N2 | 15.0 | ~12.01 (?) | | | ~1.0 (?) | | no |
| Karlovasi, K2 (Samos Isl.) | 17.0 | ~11:59 (+) | | | ≥0.7 (+) | ≥84 (+) | yes |
| Karlovasi, K3 (Samos Isl.) | 17.5 | 11:57:30 (−)<br>11:59:30 (+) | | | ~1.0 (−)<br>1.80(+) | ~15 (−)<br>53 (+) | yes |
| A. Nikolaos, K4 (Samos Isl.) | 12.0 | 11:53:10 (−)<br>11:55:36 (+)<br>11:55:42 (+) | | | ~1.0 (-)<br>1.2 (+)<br>3.55 (+) | ~15 (−) | yes |
| Evdilos Port, I1 (Ikaria Isl.) | 64.0 | ~12:02 (−)<br>~12:04 (+)<br>~12:28 (+) | | | 0.70 (+)<br>~0.70 (+) | ~10 (−) | no<br>no |
| A. Kirykos, I3 (Ikaria Isl.) | 56.0 | ~12:04 (−)<br>~12:10 (+)<br>~12:43 (+) | | | ~1.0 (+)<br>~1.0 (+) | ~10(-) | no<br>no |

**Table 2.** *Cont.*

| Observation Site | Δ (km) | t (UTC) | h (m) | d(m) | $h_{max}$(m) | $d_{max}$(m) | dam |
|---|---|---|---|---|---|---|---|
| Komi, O1 (Chios Isl.) | 75.0 | ~12:35 (−) ~12:40 (+) | | | ~1.00 (+) | ~15 (−) ~20 (+) | yes |
| Nimporio, O3 (Andros Isl.) | 165.0 | ~12:50 (+) | | | 0.55 (+) | | no |

**Table 3.** Tsunami observations at western Turkey localities for cases of estimated run-up > 0.5 m, after [2]: $\varphi^oN$ = geographic latitude, $\lambda^oE$ = geographic longitude, other symbols as in Table 2.

| Locality | $\varphi^oN$ | $\lambda^oE$ | Δ (km) | t (UTC) | $h_{max}$ (m) | Polarity | dam |
|---|---|---|---|---|---|---|---|
| Zeytineli | 38.19600 | 26.48859 | | | 1.9 | | yes |
| Dermicily | 38.210438 | 26.694419 | | ~12.14 | 0.7 | (−) | yes |
| Sigacik | 38.201305 | 26.785967 | | | 1.5 | | yes |
| Akarca | 38.1647 | 26.8146 | | ~12.03 | 1.3 | (−) | yes |
| Tepecik | 38.1355660 | 26.8330510 | | | 1.5 | | no |

## 3. Results

### 3.1. Tsunami Attenuation

The data collected make it possible to examine the decay of the tsunami wave height, h, as a function of epicentral distance, Δ. Far-field data are available from seven tide-gauge records operating at epicentral distances ranging from 112 to 286 km (Figure 1, Table 4). At closer distances, however, no tide records are available. Therefore, we assumed that the run-up values measured in the field could be considered as a proxy of the wave height. Since the uncertainty involved in run-up values of less than 0.5 m is relatively high, we considered values larger than 0.5 m. The run-up values taken into account from both the Greek islands and the western Turkey localities are listed in Tables 2 and 3, respectively.

**Table 4.** Data set used to calculate tsunami magnitude, $M_t$, for the $M_w$ = 7.0 earthquake of 30 October 2020 from tsunami height, h, recorded at 7 tide stations situated at epicentral distances Δ. h is taken as half of the maximum crest-to-trough height. Stations are operated by the following agencies: 1 by the Turkish General Command Mapping (TGCM); 2,3,4 jointly by the Space, Security and Migration Directorate-Joint Research Center at Ispra (JRC, EC) and the National Observatory of Athens (NOA, Greece), IDSL = Inexpensive Device for Sea Level Measurement; 5 by the Hellenic Navy Hydrographic Service (HNHS, Greece); 6,7 by NOA. Tide records were retrieved from the JRC World Sea Levels platform (https://webcritech.jrc.ec.europa.eu/) and the Sea Level Station Monitoring Facility of the IOC (http://www.ioc-sealevelmonitoring.org).

| No. | Tide Station | Lat° N | Lon° E | Δ (km) | H (m) |
|---|---|---|---|---|---|
| 1 | BODRUM, TGCM | 37.03217 | 27.423453 | 112 | 0.03 |
| 2 | KOS, IDSL-25 | 36.898362 | 27.287792 | 118 | 0.095 |
| 3 | KOS-MARINA, IDSL-33 | 36.891013 | 27.303632 | 120 | 0.09 |
| 4 | PLOMARI, IDSL-41 | 38.97188 | 26.37055 | 122 | 0.05 |
| 5 | SYROS, HNHS | 37.438 | 24.9411 | 174 | 0.05 |
| 6 | KASOS, NOA-03 | 35.4186 | 26.92184 | 274 | 0.06 |
| 7 | HERAKLION, NOA-10 | 35.3484 | 25.15254 | 286 | 0.08 |

Transformation of the power-law formulas shown in Figure 31 provides

$$\log h = 1.51 - \log \Delta \quad (1)$$

for all field and tide data considered together, and

$$\log h = 0.84 - 0.50 \log \Delta \quad (2)$$

for only field data. Similar formulas with exponents of almost unity have been found for Japanese tsunamis [19] as well as for large Pacific Ocean tsunamis [20]. In the 1980s, a similar formula was proposed for Greek tsunamis under the assumption that in the epicentral area ($\Delta_o$ = 30 km) no wave attenuation occurs [21]:

$$\log h = 5.25 - 2.35 \log (\Delta + \Delta_o) \quad (3)$$

Comparison of Formulas (1)–(3) and their implications are discussed later.

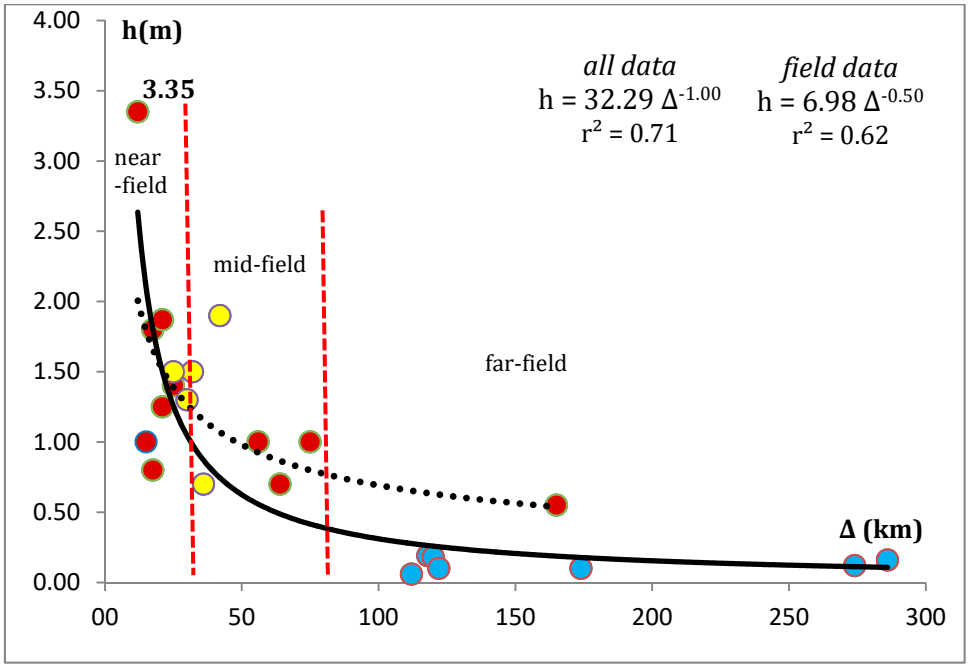


**Figure 31.** Decay of tsunami wave height, h, versus epicentral distance, Δ. Three independent data sets have been used: (i) maximum run-up measured in Greek islands (brown circles, present study), (ii) maximum run-up measured in western Turkey localities (yellow circles, [2]), (iii) wave heights measured in far-field tide records (blue circles, present study); run-up measured in the field is considered as a proxy of h (Tables 2 and 3). Best fit curves for all data (solid) and for only field data (i) and (ii) (dashed) show power-law decay of h; r is correlation coefficient.

### *3.2. Tsunami Run-Up Timeline*

We combined video record analysis and field inspection to plot the tsunami run-up timeline in the east coast of Vathy bay (Figure 32) and in site K4, in the north coast of Samos (Figure 33). Data for Vathy bay were taken from the sites V1 and V4 where the most accurate video records are available. The videos made it possible to control the run-up timeline in the coastal zone at a run-in distance of d = 35 m where the second inundation caused a run-up h = 1.4 m asl, which is higher than the h = 1.15 m found for the first inundation. This result is consistent with the accounts of many eyewitnesses who reported that the second wave was stronger in relation to the first. The elapsed time between the inception of each inundation phase and the occurrence of the respective maximum run-up at d = 35 m was ~2 min.

In site K4, a detailed reconstruction of the sea level changes has been possible thanks primarily to the video record from the security camera shooting very close to the shore. Additional information was collected from the local residents who experienced the tsunami attack by themselves. After an initial leading phase of sea recession occurring in less than 2 min from the earthquake, the main sea level rise arrived only ~40 s from the occurrence of a second minor sea recession and in ~4 min from the earthquake origin time. The maximum wave height value was measured at 3.35 m in the house or 2.80 outside of it. A second important sea level rise of ~1.60 asl occurred at K4 around 12.15.

The fact that the wave arrived in such a short time with such a large height is discussed later. A characteristic difference of the two phases of sea level rise has been that the first moved obliquely to the beach while the second was a nearly uniform sea level rise along the entire beach length. These peculiarities of the wave form are discussed later.

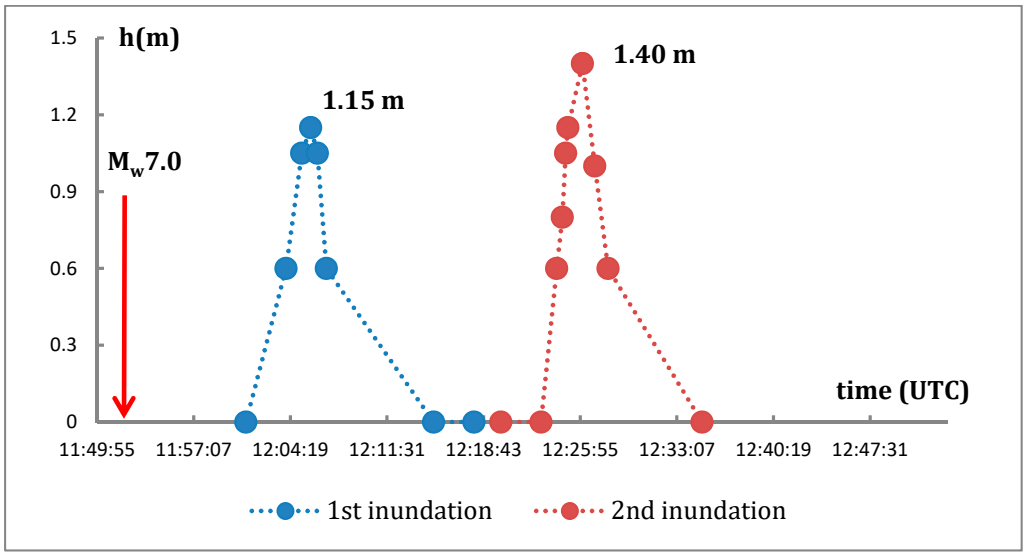


**Figure 32.** Timeline of the tsunami run-up estimated from video records and field inspection at run-in distance d = 35 m in Vathy east coast near transect 1 between the observation sites V1 and V4 (Figure 4). Datum 0 m is the sea level, ground level is at 0.6 m asl. Red arrow shows earthquake origin time, $M_w$ is moment magnitude. For maximum run-up measured further inland up to d~100 m, see in text and Figure 4.

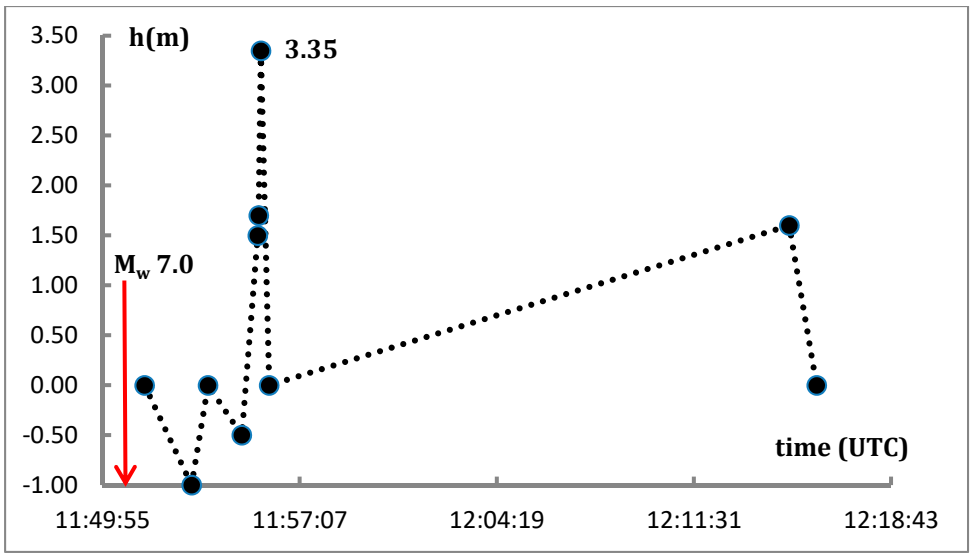


**Figure 33.** Site K4. Timeline of the tsunami height, h, based on video record and eyewitness accounts; h is estimated relative to sea level 0 m (datum); house entrance level at 1.5 asl. Red arrow shows earthquake origin time; $M_w$ is moment magnitude. Two sea recession phases occurred before major sea level rise.

### *3.3. Tsunami Source Properties*

#### 3.3.1. Tsunami Magnitude

Although several efforts have been made for the establishment of tsunami magnitude scales, no standard method has been introduced so far (see review in [22]). One of the most

promising approaches is based on Pacific Ocean data [20] and uses Formula (4) to calculate the tsunami magnitude, $M_t$, where h (in m) is the maximum wave heights at nearshore tide-gauge records at epicentral distances, Δ (in km):

$$M_t = \log h + \log \Delta + 5.80 \quad (4)$$

The constant in (4) has been obtained under the requirement $M_t = M_w$ on the average for the calibration data set used in [20]. $M_t$ represents not only the overall physical size of a tsunami but also the seismic moment magnitude, i.e., the size of the tsunamigenic earthquake. In the Mediterranean Sea basin, the applicability of this approach was for the first time tested with success after the earthquakes of 25 October 2018 ($M_w$ = 6.8) and 2 May 2020 ($M_w$ = 6.6) that ruptured along the Hellenic arc [22,23]. $M_t$ of 7.0 and 6.8 was calculated for the 2018 and 2020 events, respectively.

We applied this method to the Samos tsunami, taking available wave heights as recorded in seven mareograms (Table 4). We found $M_t$ = 6.8, which is close to $M_w$ = 6.9 or $M_w$ = 7.0 calculated independently from seismic records. The difference is relatively small and might be attributed to several factors including the lack of wave height data from near-field tide records. From the power-law decay of the run-up field data sets (Figure 31), we were motivated to also test field data for $M_t$ calculation. The test proved quite successful given that $M_t$ = 7.1 and $M_t$ = 7.0 was found from field data alone and from field and tide data considered together, respectively.

#### 3.3.2. Tsunami Source Area and Displacement Amplitude

The tsunami source area, S, and the displacement amplitude, α, of the oceanic surface at the source are two important parameters for further understanding the tsunami event. A series of empirical relationships help to calculate S and α. Usually, S is taken to be equal either to the fault area or to aftershock area. From global data of shallow earthquakes of $M_w \geq 6.5$, a scaling relation between seismic moment $M_o$ and fault area has been found [24]. However, from the empirical relationship A1 (Appendix B) [25] among mean radius, $R_{TS}$, of the tsunami source area, and $M_w$, it results that S is several times larger than the fault area at the earthquake source. For a circular tsunami source and $M_w$ = 7.0, the relationship A1 returns $R_{TS}$ = 25 km and S = 1960 km$^2$. The empirical relationships A2 and A3, found between $M_w$ and the aftershock area for the Mediterranean Sea [26] and global [27] earthquakes, for $M_w$ = 7.0, yield aftershock areas of 1260 km$^2$ and 741 km$^2$, respectively. Through a preliminary relocation of the aftershock sequence until 8 November 2020, it comes out that the aftershock activity is spatially distributed in two distinct clusters [28]. Considering the two clusters together, including the area between them, we calculated that the aftershock cloud area is no more than 900 km$^2$, which underestimates the tsunami source area by more than a factor of 2.

The global empirical relationship A4 [25] allows calculation of the displacement amplitude, α, of the oceanic surface at the source from $M_w$. On the other hand, A5 [27] provides the average fault displacement from $M_w$. For the Samos tsunami, A4 and A5 return α = 1 m and α = 0.91 m, respectively. These results are consistent with the wave heights observed around the source in the islands of Samos, Ikaria and Chios (sites, N1,N2,K2,I1,I3,O1) and in western Turkey sites (Dermicily, Sigacik, Akarca, Tepecik). However, in some observation sites, such as Vathy, Karlovasi port and Zeytineli, the wave height reached up to ~2 m, very likely due to resonance effects in bays and ports. The Ayios Nikolaos case (site K4), however, makes an important exception since extreme wave height was observed there in a coastal stretch that does not favor wave amplification. This exceptional case is recalled later.

### *3.4. Tsunami Impact*

The Samos tsunami has been a moderate event that caused material damage indoor and outdoor at epicentral distances of less than 80 km, i.e., in the near- and mid-field domains (Tables 2 and 3, Figure 34). The affected coastal segments include north Samos,

southeast Chios as well as western Turkey localities to the north and northeast of the source. In all damaged sites, the wave run-up has been ~1 m or more. No damage was reported from areas with smaller run-up. Only one fatality was reported in western Turkey [2]. No structural damage to buildings was observed due to the tsunami.


**Figure 34.** Main tsunami features in the Greek islands of Samos, Ikaria, Chios and Andros (present study) and in western Turkey localities (after [2]); data in Tables 2 and 3. Star illustrates the 30 October 2020 earthquake epicenter. The three rows in each panel show polarity (top), arrival time of leading wave (in minutes after earthquake, mid) and maximum run-up, h (in m, bottom). A locality is represented in the map only if h > 0.5 m. Signs + and - stand for leading sea rise and recession, respectively. Lack of a row reflects lack of data. Panel in red or beige shows locality damaged or not damaged by the tsunami, respectively. Tsunami damage was extended in an area of ~4000 km$^2$.

In north Samos, the main damage was caused in both sides of the Vathy bay, in the port and marina area of the Karlovasi town and in the Ayios Nikolaos settlement. In the east Vathy bay and in Karlovasi, damage was mainly noted in cars and small boats as well as in houses, offices, hotel lobbies, shops, restaurants, cafes and other stores, all situated at the ground level up to ~100 m maximum run-in distance. Similar types of damage were observed in the localities of Zeytineli, Sigacik, Akarca and Tepecik of western Turkey [2]. In the west Vathy bay (Malagari settlement, V8), limited indoor damage was reported while a small boat was lost in the sea. A big iron container with an estimated weight of ~10 t was moved from its initial position. In the Ayios Nikolaos settlement (K4), minor indoor damage was caused in a couple of households, while a few small boats were either damaged or lost in the sea. In south Chios Island, a few small boats were damaged too.

## 4. Discussion

The tsunami caused by the large Samos earthquake of 30 October 2020 in the eastern Aegean Sea has been a quite challenging event from several perspectives. It has been a characteristic very near-field tsunami given that the first inundation arrived at the closest settlement within only 4 min from the earthquake origin time. The tsunami was recorded

only at distant tide-gauge stations due to a lack of stations in the near-field domain. Thus, the 2020 Samos tsunami underlined the gap existing in the tide-gauge network in the Aegean Sea and in the largest part of the Mediterranean region. The need to densify the sea level monitoring system in the eastern Mediterranean was noted recently after the earthquake ($M_w$ = 6.6) and tsunami event of 2 May 2020 near Crete [29].

The data sets collected are heterogeneous since they come from a variety of sources including field surveys, video records, far-field mareograms, eyewitness accounts and communications with local authorities. However, thanks to the combined analysis of the various data sets we have been able to resolve the arrival times, polarity modes and amplitudes of the leading waves and of the inundation phases, to measure run-up and run-in values in several localities as well as to estimate tsunami source parameters, such as magnitude, source area, displacement amplitude and the wave attenuation. The main tsunami features are summarized in Figure 34. In the most important observation sites (Vathy, Karlovasi, Ayios Nikolaos), for the wave arrival times the error is within only a few seconds since they are based on accurate video records. Run-up height measurements are also based on the combined analysis of the various types of data sets. In the most important sites, the error involved in run-up height is in the order of a few centimeters. For some less important observation sites, however, our estimations of run-up heights of less than ~0.5 m have been based on eyewitness accounts and, therefore, suffer from relatively large error.

In most observation points around the source, the leading wave has been a sea recession, which is well documented in the NW Samos and westwards up to Ikaria Isl. (Figure 34). Sea recession was reported as the first motion in western Turkey as well, although there is a lack of data in some of the coastal spots examined [2]. Sea recession as a predominant mode of first wave motion is an evidence that the tsunami was produced by a unipolar disturbance, i.e., seismic fault displacement. However, sea rise has been reported as first wave motion in the 5-km-long V-shaped Vathy bay, NE Samos coast. One may argue that this perhaps reflects the lack of leading wave observations. It would be strange enough that a sea recession occurring in the bay of Vathy town at noon time during a nice calm day passed unnoticed. On the other hand, one may not rule out that although the initial motion was a recession, it appeared to be an advance possibly due to reflection and/or refractions occurring in the bay, particularly near its mouth, before the sea disturbance arrived with significant amplified sea rise in the bay head.

The displacement amplitude of 1 m found in the tsunami source area is consistent with the wave height measured in several observation sites around the source. In ports and closed bays, however, this height was exceeded, very likely due to resonance effects. In site K4, north Samos, at the shortest epicentral distance ($\Delta$~12 km) and at the shortest arrival time (~4 min) we measured an extreme height value of h~3.35 m asl, or, more conservatively, of 2.80 m asl at minimum. A few kilometers to the west and east of K4, at comparable epicentral distances (sites N1, N2, K2 at $\Delta$ of 17.5, 15, 16.5 km, respectively) the h values have been around 1 m asl. In K3, Karlovasi port ($\Delta$~17 km), h did not exceed 1.8 m asl. Consequently, the extreme wave height at K4 needs explanation.

The short time arrival at K4 is explainable by the short epicentral distance. From a bathymetry map of the area [30] it results that in the epicentral area the sea depth is ~400 m, which gradually decreases towards the Samos north coast. For an average z = 200 m and assuming that the wave velocity is equal to $(gz)^{1/2}$, where g is the gravity acceleration, we get a theoretical wave arrival time at K4 equal to 4.4 min.

The theoretical arrival time found is absolutely consistent with the observed arrival time (4 min) of the major sea level rise recorded at the video available for K4. However, wave amplification does not account for the extreme height since the site K4 is not a closed bay. A possible key to explain the extreme height may rely on that the extreme wave phase moved obliquely to the beach as it is clearly recorded in the video. On the contrary, the eyewitness reported that the second major wave of h~1.60 asl occurred around 12:15 as a quasi-uniform sea level rise along the beach. Such an oblique wave motion was observed in the case of the September 28th 2018 near-field tsunami in Palu-Sulawesi,

Indonesia [31]. The important role of landslides in such tsunami characteristics has been well documented [31,32]. We do not rule out that a submarine landslide triggered by the Samos earthquake between the source and the north Samos coast may have been coupled with the broadside tsunami, thus resulting in the extreme wave height observed in Ayios Nikolaos at site K4. During our post-tsunami field survey, we observed subaerial, coastal landslides caused by the earthquake to the east of K4 [1,3] (Figure 35). The significantly lower tsunami height observed to the east and west of K4 is consistent with the rapid quasi-exponential attenuation of wave heights with distance from the landslide source due to strong wave dispersion found from a global data set of tsunamis triggered by landslides [33].

(**a**) (**b**)

**Figure 35.** Coastal landslide caused by the Samos earthquake in the Avlakia site a few kilometers to the east of site K4 (**a**). The landslide is tectonically controlled by a normal fault striking NW–SE and dipping to NE (**b**) (photos credit, G.A. Papadopoulos).

An alternative explanation for the extreme height is that a near-field edge wave phase arrived at K4. Near-field tsunami edge waves are on-shelf trapped waves propagating along the shelf with a dispersive attenuation [34–36]. Such waves are distinguished from broadside waves that are local waves propagating directly from the source in a direction approximately perpendicular to the strike. The largest local run-up is usually caused by broadside waves. For landslide tsunamis, however, the maximum edge-wave amplitude can exceed the maximum broadside amplitude [37]. Both alternatives proposed to explain the extreme wave height at K4 call for challenging future research.

The Samos tsunami magnitude $M_t = M_w$~7.0 has been calculated from wave heights. The tsunami magnitude obtained in this study as well as those obtained in other recent tsunamis [22,23] are consistent with the magnitudes determined independently from seismic records. This implies that the method used is a promising approach for the development of a tsunami magnitude scale in the Mediterranean Sea. All evidence suggests that the Samos tsunami has been the largest event occurring in the Mediterranean since the large tsunami of 9 July 1956 in the south Aegean Sea. The tsunami caused by the Boumerdès-Zemmouri (Algeria) 2003 earthquake of $M_w = 6.9$ in the western Mediterranean basin [38] is likely comparable to that of Samos.

The study of the 2020 Samos tsunami provides, for the first time in the eastern Mediterranean, data accurate enough to reliably approach the tsunami attenuation in terms of height (h) decay as a function of epicentral distance (Figure 31). The decay of h is faster according to Formula (1) as compared to the decay predicted from Formula (2). This is due to the field data having been available only in the near-field and mid-field domains, i.e., at $\Delta < 80$ km, with the exception of only one value taken at $\Delta = 165$ km. On the contrary, Formula (2) was found using not only field data but also far-field data from tide-gauge

records. On the other hand, the Formula (3), which is based on old data of low accuracy, overestimates the wave height in relation to (1) for $\Delta > 40$ km and in relation to (2) for all $\Delta$ values. The reason is that the Formula (3) has been produced assuming that no height decay occurs in the near-field domain ($\Delta_o = 30$ km). This assumption was adopted very likely due to the low accuracy of the near-field data used by the authors [21] proposing the Formula (3). However, the present study as well as the studies of other recent tsunamis [22,23] showed that the tsunami height decays even in the very near-field domain.

The 2020 Samos earthquake and tsunami came after the strong earthquakes of 12 June 2017 ($M_w = 6.3$) and of 20 July 2017 ($M_w = 6.6$) [39] occurring in the areas of Lesvos and Bodrum-Kos, respectively (Figure 1). All three events have been tsunamigenic and of similar focal mechanisms with normal faulting trending ~E–W but the Samos tsunami has been the largest among the three. In view of the low historical tsunami record in the east Aegean Sea, the new light shed by the three recent tsunami events calls for reexamination of the tsunami hazard level in the area.

Of particular interest is the co-seismic uplift by ~15–25 cm observed in several coastal spots of the island of Samos [1,3]. Tectonically, such a displacement has been anticipated since Samos is lying on the footwall domain of the causative normal fault, if it dips northwards [4,28]. An extensive investigation of the Samos co-seismic uplift is on the way by our research team. From the tsunami impact point of view, it is noteworthy that the coastal uplift reduced the tsunami inundation and run-up height with respect to those expected if no coastal uplift had happened before the tsunami arrival.

The civil protection response to the Samos tsunami is a quite remarkable issue. Although it is beyond of the scope of this paper, a note is needed since it has been the first time in the European-Mediterranean region that the tsunami warning message reached the general public regardless the effectiveness of the warning. The inability of civil protection authorities to warn the general public in case of a tsunami in the Mediterranean region has been already noted and discussed [10,23,40,41].

## 5. Conclusions

The 2020 Samos tsunami was an important event from several perspectives. First, it was the largest tsunami in the eastern Mediterranean, if not in the entire Mediterranean basin, since the occurrence of the large tsunami observed after the $M_w = 7.7$ earthquake of 9 July 1956 in the south Aegean Sea. In addition, it was a characteristic near-field event with the maximum sea level rise arriving at the shortest epicentral distance ($\Delta$~12 km) in Ayios Nikolaos settlement, on the north coast of Samos, within only ~4 min. Considering the average sea depth of ~200 m between the epicenter and Ayios Nikolaos, the theoretical arrival time was found to be equal to 4.5 min.

In most observation sites around the source, including Samos north coast, Ikaria Island and western Turkey localities, the leading wave has been a sea recession, implying that there was tsunami generation mechanism due to seismic dislocation. The wave heights measured around the source have been ~1 m, which is consistent with the estimated displacement amplitude at the tsunami source. The wave height reached up to around 2 m only in bays and ports, such as in Vathy and Karlovasi, north Samos, and in a couple of western Turkey localities. In the bay of Vathy town, an initial sea recession has not been reported. Two inundation phases, with arrival times of 13 min and 19 min after the earthquake, have been documented from field observations, video records and eyewitness accounts. The second inundation was the strongest with a measured run-up of 2.0 m asl at inundation distance d~100 m. However, a sea recession as the first wave motion cannot be excluded, but was not observed in the bay for various reasons. In several localities of the south coast of Samos, the wave height of ~0.5 m or less was observed.

In Ayios Nikolaos, a measured extreme wave height of 3.35 m asl, or more conservatively of 2.80 m asl, needs explanation. A key element is that the powerful wave motion was oblique along the beach, as is clearly seen in an accurate video record. This is similar to the 2018 Palu-Indonesia tsunami produced by a coupling of seismic and landslide tsunamis. In

Samos, the seismic tsunami coupled with a tsunami produced by a small scale submarine landslide may explain the extreme tsunami height measured in Ayios Nikolaos.

From several video records, we estimated wave velocity gradually decreasing from offshore north Samos (23 m/s), along the north Samos beach (7.8 m/s) and in the Vathy bay (3.3 m/s). Even smaller velocity was estimated on land during the upstream water motion. In Vathy, it was found to be ~0.8 m/s for the first inundation and from 0.92 m/s to 1.4 m/s for the second inundation. From the run-up values obtained, little doubt remains that the tsunami was amplified in ports and narrow bays. However, we found a power-law decay of the wave height away from the source. Empirical Formula (1) is very likely the most reliable proposed so far in the Mediterranean basin for the wave height decay of seismic tsunamis.

Wave heights measured at seven far-field mareograms returned tsunami magnitude $M_t = M_w = 6.8$, which is a good approximation of the earthquake magnitude calculated independently from seismic records. Even better results were obtained by considering wave height from field data only ($M_t = 7.1$) and wave height from field data and mareograms taken altogether ($M_t = 7.0$). The successful $M_t$ estimation not only of the Samos 2020 tsunami, but also of other recent events, indicates that the development of a tsunami magnitude scale in the Mediterranean basin is a realistic goal. The tsunami source area was found to be equal to about 1960 $km^2$, which doubles the aftershock area. This result is consistent with results based on global data sets.

The tsunami caused material damage in cars, in small vessels and in various coastal stores, offices, hotel lobbies, restaurants and other tourist and commercial shops, particularly in Vathy and Karlovasi in Samos Isl. as well as in western Turkey localities. However, no structural damage to buildings was observed because of the tsunami. A few small boats were damaged or lost in the sea. In several observation sites, fishes, sand, pebbles, salt and extensive littering was left behind by the wave. In at least one coastal spot, the tsunami withdrawal caused local ground erosion. In south Chios Island, small vessels were damaged. It is noteworthy that damage was observed in sites with wave run-up of ~1 m asl or more. No damage was caused with run–up values of less than 1 m. Tsunami damage was extended in an area of ~4000 $km^2$ around the seismic source, which is about twice the tsunami source area.

The mortality caused by the tsunami has been nearly zero since only one fatality was reported in western Turkey. This is because the wave height and run-up have not been large enough to cause massive casualties. According to coastal field observations, the island of Samos very likely uplifted co-seismically with amplitude varying from ~0.15 m to ~0.25 m [1,3,42]. Coastal uplift may have contributed to reducing the run-up and, consequently, the impact of the tsunami wave. Further research regarding this point is a challenge. There is evidence that in both Samos and western Turkey people, to a large extent, evacuated inland immediately after the earthquake. The warning message disseminated to the general public of the eastern Aegean Sea Greek islands may have also contributed to protecting people from the second inundation in Vathy town.

Low tsunami hazard has been considered so far in the eastern Aegean Sea area. However, the Samos 2020 tsunami is the third occurring in the area in recent years after the tsunamis caused by strong earthquakes occurring on 12 June 2017 ($M_w = 6.3$) and 20 July 2017 ($M_w = 6.6$) to the north and south of Samos, respectively. These tsunami waves, although have been of only local impact, call for a reevaluation of the tsunami hazard level and the preparedness for tsunami risk mitigation in the area.

**Author Contributions:** Conceptualization, I.T., E.L. and G.A.P.; methodology, I.T., E.L. and G.A.P.; investigation, I.T., M.G., S.M., E.L., G.A.P., and M.T.; resources, E.L.; data curation, M.G., S.M., and M.T.; writing—original draft preparation, I.T.; writing—review and editing, I.T., M.G., S.M., E.L., and G.A.P.; supervision, E.L., G.A.P. All authors have read and agreed to the published version of the manuscript.

**Funding:** This research of I.T. was funded by the Hellenic Foundation for Research and Innovation (HFRI) and the General Secretariat for Research and Technology (GSRT), under HFRI PhD Fellowship grant (GA. no. 490).

**Institutional Review Board Statement:** Not applicable for studies not involving human or animals.

**Informed Consent Statement:** Not applicable for studies not involving human.

**Data Availability Statement:** The data presented in this study are available in Tables 2–4.

**Acknowledgments:** This paper is a contribution to the Post-Graduate Program "Environmental, Disaster, and Crises Management Strategies," Department of Dynamic, Tectonic and Applied Geology, Faculty of Geology and Geoenvironment, National and Kapodistrian University of Athens, Greece, which supported the post-event field survey. IT was supported by the Hellenic Foundation for Research and Innovation (HFRI) and the General Secretariat for Research and Technology (GSRT), under the HFRI PhD Fellowship grant (GA. no. 490). IT and GP contributed to the European Cooperation in Science and Technology COST project "AGITHAR-Accelerating Global science In Tsunami HAzard and Risk analysis". The field trip of GP was supported by the "Safe Greece" Organization and his research contribution was performed in the frame of the "International Society for the Prevention and Mitigation of Natural Hazards (Natural Hazards Society)". Special thanks are due to our collaborators Nikos Vorias, civil protection officer in Chios, for his kind help to collect observations about the tsunami impact in Chios, and to Nikos Mourtzas and Eleni Kolaiti, "AKTES-Society for the Study of Ancient Coastlines", for providing tsunami information, a video record of the tsunami inundation and measurement of the pier level in Nimporio bay, Andros Island. Mr Manolis Pirgiotis and Mr Dimitris Kasmirlis provided videos from security cameras in the Library building and Hertz office, Vathy town, respectively. Mrs Cornilia Papakonstantinou, owner of the video at site K4, provided important information about the tsunami behavior and its impact at that site. We are thankful to all of them. Thanks are also due to officers in the port and civil protection authorities in Samos and Ikaria islands as well as to a large number of earthquake and tsunami eyewitnesses (see text and photo credits) and journalists in Samos, Chios and Ikaria islands who provided valuable information. We appreciate the critical reading of an early manuscript version by Alessandro Annunziato, JRC/EC, Ispra. Thanks are due to A.C. Yalciner, Middle East Technical University, Ankara, for providing an early version of the report about the post-tsunami survey in west Turkey and for exchanging opinions about the tsunami measurements there.

**Conflicts of Interest:** The authors declare no conflict of interest.

## Appendix A

Earthquake focal parameters listed in Table 1 have been retrieved from the following sources, all accessed on 25th November 2020: GCMT Project (https://www.globalcmt.org/CMTsearch.html); NOA (https://bbnet.gein.noa.gr/HL/seismicity/mts/revised-moment-tensors); EMSC (https://www.emsc-csem.org/Earthquake/263/M7-0-DODECANESE-ISLANDS-GREECE-on-October-30th-2020-at-11-51-UTC); GFZ (https://geofon.gfz-potsdam.de/old/eqinfo/list.php?Page=4); USGS (https://earthquake.usgs.gov/earthquakes/eventpage/us7000c7y0/executive).

## Appendix B

The empirical relation A1 between the mean radius, $R_{TS}$, of the tsunami source area and $M_w$ was found [25] to be:

$$\log R_{TS} = (0.50 \pm 0.07)\, M_w - (2.10 \pm 0.6) \quad \text{(A1)}$$

From Mediterranean earthquake data, it has been found that the rupture area, RA, is a function of the earthquake magnitude according to the next relationship [26]:

$$\log RA = (0.81 \pm 0.06)\, M_w - (2.57 \pm 0.43) \quad \text{(A2)}$$

The relationship A3 was found [27] among RA and Mw for global data set of normal earthquakes:

$$\log RA = (-2.87 \pm 0.5)\, M_w - (0.82 \pm 0.08) \quad (A3)$$

The dependence of displacement amplitude, $\alpha$, at the tsunami source on $M_w$ of tsunamigenic earthquakes is [25]:

$$\log \alpha = (0.80 \pm 0.1)\, M_w - (5.6 \pm 1.0) \quad (A4)$$

Both A1 and A4 are valid for a global earthquake data set of $6.7 < M_w < 8.5$.

From global data set of normal earthquakes, it has been found that the average fault displacement, A, depends on the magnitude as follows [27]:

$$\log RA = (0.81 \pm 0.06)\, M_w - (2.57 \pm 0.43) \quad (A5)$$

## References


1. Triantafyllou, I.; Gogou, M.; Mavroulis, S.; Katsetsiadou, K.-N.; Lekkas, E.; Papadopoulos, G.A. *The Tsunami Caused by the 30 October 2020 Samos (Greece), East Aegean Sea, Mw6.9 Earthquake: Impact Assessment from Post-Event Field Survey and Video Records*, Version 2 ed; Department of Dynamic, Tectonic & Applied Geology, Faculty of Geology & Geoenvironment, National & Kapodistrian University of Athens: Athens, Greece, 2020; Report; p. 20. [CrossRef]
2. Yalciner, A.C.; Dogan, G.G.; Ulutaş, E.; Polat, O.; Tarih, A.; Yapa, E.R.; Yavuz, E. The 30 October 2020 (11:51 UTC) Izmir-Samos Earthquake and Tsunami: Post-Tsunami Field Survey Preliminary Results. Report. 3 November 2020, p. 28. Available online: https://drive.google.com/file/d/1HzVFjMsZ5zei2UTAoIdrcWFtPpzGr8U9/view (accessed on 17 November 2020).
3. Lekkas, E.; Mavroulis, S.; Gogou, M.; Papadopoulos, G.A.; Triantafyllou, I.; Katsetsiadou, K.-N.; Kranis, H.; Skourtsos, E.; Carydis, P.; Voulgaris, N.; et al. The October 30, 2020 $M_w$6.9 Samos (Greece) earthquake. In *Newsletter of Environmental, Disaster and Crises Management Strategies*; Department of Dynamic, Tectonic & Applied Geology, Faculty of Geology & Geoenvironment, National & Kapodistrian University of Athens: Athens, Greece, 2020; Volume 21, p. 156, ISSN 2653-9454. [CrossRef]
4. Ganas, A.; Elias, P.; Briole, P.; Tsironi, V.; Valkaniotis, S.; Escartin, J.; Karasante, I.; Efstathiou, E. Fault responsible for Samos earthquake identified. *Temblor* **2020**. [CrossRef]
5. Mountrakis, D.; Kilias, A.; Vavliakis, E.; Psilovikos, A.; Karakaisis, G.; Papazachos, C.; Thomaidou, E.; Seitanidis, G. *Neotectonic Map of Greece, "Samos" Sheet, Scale 1:75.000*; Institute of Geology and Mining Exploration: Athens, Greece, 2006.
6. Pavlides, S.; Tsapanos, T.; Zouros, N.; Sboras, S.; Koravos, G.; Chatzipetros, A. Using Active Fault Data for Assessing Seismic Hazard: A Case Study from NE Aegean Sea, Greece. In Proceedings of the XVIIth International Conference on Soil Mechanics and Geotechnical Engineering, Alexandria, Egypt, 2–3 October 2009.
7. Chatzipetros, A.; Kiratzi, A.; Sboras, S.; Zouros, N.; Pavlides, S. Active faulting in the north eastern Aegean Sea Islands. *Tectonophysics* **2013**, *597–598*, 106–122. [CrossRef]
8. Greek Database of Seismogenic Sources. Available online: http://gredass.unife.it/gredassGM/ (accessed on 24 December 2020).
9. Papadopoulos, G.A.; Gràcia, E.; Urgeles, R.; Sallares, V.; De Martini, P.M.; Pantosti, D.; González, M.; Yalciner, A.C.; Mascle, J.; Sakellariou, D.; et al. Historical and pre-historical tsunamis in the Mediterranean and its connected seas: Geological signatures, generation mechanisms and coastal impacts. *Mar. Geol.* **2014**, *354*, 81–109. [CrossRef]
10. Papadopoulos, G.A. *Tsunamis in the European-Mediterranean Region: From Historical Record to Risk Mitigation*; Elsevier: Amsterdam, The Netherlands, 2016; p. 271. ISBN 987-0-12-4202245.
11. Ambraseys, N.N. *Earthquakes in the Mediterranean and Middle East, a Multidisciplinary Study of Seismicity up to 1900*; Cambridge University Press: Cambridge, UK, 2009; p. 947.
12. Papazachos, B.C.; Papazachou, C. *The Earthquakes of Greece*; Ziti Publ.: Thessaloniki, Greece, 2003; p. 286. (In Greek)
13. Makropoulos, K.; Kaviris, G.; Kouskouna, V. An updated and extended earthquake catalogue for Greece and adjacent areas since 1900. *Nat. Hazards Earth Syst. Sci.* **2012**, *12*, 1425–1430. [CrossRef]
14. ISC-GEM. The ISC-GEM Global Instrumental Earthquake Catalogue, # Version 7.0-Released on 2020-04-09. 2020. Available online: http://doi.org/10.31905/D808B825 (accessed on 5 November 2020).
15. Galanopoulos, A.G. The seismic sea-wave of 9 July 1956. *Prakt. Acad. Athens* **1957**, *32*, 90–101, (In Greek with English abstract).
16. Ambraseys, N.N. The seismic sea-wave of July 1956 in the Greek Archipelago. *J. Geophys. Res.* **1960**, *65*, 1257–1265. [CrossRef]
17. Farreras, S.F. Post-Tsunami Field Survey Procedures: An Outline. In *Natural Hazards*; Papadopoulos, G.A., Murty, T., Venkatesh, S., Blong, R., Eds.; Springer: Dordrecht, The Netherlands, 2000. [CrossRef]
18. International Tsunami Survey Team (ITST). *Post-Tsunami Survey Field Guide*, 2nd ed.; IOC Manuals and Guides No. 37; UNESCO: Paris, France, 2014; p. 108.
19. Watanabe, H. Amplitude coefficient of maximum tsunami by traveling distance and tsunami magnitude. In *Tsunami '93-Proc. of the IUGG/IOC International Tsunami Symposium*; Tsuchiya, Y., Shuto, N., Eds.; Japan Society of Civil Engineers: Wakayama, Japan, 1993; pp. 271–276.

20. Abe, K. Estimate of tsunami run-up heights from earthquake magnitudes. In *Tsunami: Progress in Prediction, Disaster Prevention and Warning*; Tsuchiya, Y., Shuto, N., Eds.; Kluwer: Amsterdam, The Netherlands, 1995; pp. 21–35.
21. Papazachos, B.C.; Koutitas, C.; Hatzidimitriou, P.M.; Karacostas, B.G.; Papaioannou, C.A. Tsunami hazard in Greece and the surrounding area. *Ann. Geophys.* **1986**, *4*, 79–90.
22. Papadopoulos, G.A.; Imamura, F.; Nosov, M.; Charalampakis, M. Tsunami magnitude scales. In *Geological Records of Tsunamis and Other Extreme Waves*, 1st ed.; Engel, M., Pilarczyk, J., May, S.M., Brill, D., Garrett, E., Eds.; Elsevier: Amsterdam, The Netherlands, 2020; pp. 33–45. ISBN 978-0-12-815686-5.
23. Papadopoulos, G.A.; Lekkas, E.; Katsetsiadou, K.-N.; Rovythakis, E.; Yahav, A. Tsunami Alert Efficiency in the Eastern Mediterranean Sea: The 2 May 2020 Earthquake (Mw6.6) and Near-Field Tsunami South of Crete (Greece). *GeoHazards* **2020**, *1*, 5. [CrossRef]
24. Kanamori, H.; Brodsky, E. The physics of earthquakes. *Rep. Prog. Phys.* **2004**, *67*, 1429–1496. [CrossRef]
25. Levin, B.; Nosov, M. *Physics of Tsunamis*; Springer: Berlin/Heidelberg, Germany, 2009; p. 327. ISBN 978-1-4020-8855-1.
26. Konstantinou, K.I.; Papadopoulos, G.A.; Fokaefs, A.; Orphanogiannaki, K. Empirical relationships between aftershock area dimensions and magnitude for earthquakes in the Mediterranean Sea region. *Tectonophysics* **2005**, *403*, 95–115. [CrossRef]
27. Wells, D.L.; Coppersmith, K.J. New empirical relationships among magnitude, rupture length, rupture width, rupture area, and surface displacement. *Bull. Seismol. Soc. Am.* **1994**, *84*, 974–1002.
28. Papadimitriou, P.; Kapetanidis, V.; Karakonstantis, A.; Spingos, I.; Kassaras, I.; Sakkas, V.; Kouskouna, V.; Karatzetzou, A.; Pavlou, K.; Kaviris, G.; et al. Preliminary Report on the Mw=6.9 Samos Earthquake of 30 October 2020. Available online: https://www.emsc-csem.org/Doc/Additional_Earthquake_Report/915787/Samos2020_preliminary-report_nkua.pdf (accessed on 30 November 2020).
29. Wang, Y.; Heidarzadeh, M.; Satake, K.; Mulia, I.E.; Yamada, M. A tsunami warning system based on offshore bottom pressure gauges and data assimilation for Crete Island in the Eastern Mediterranean Basin. *J. Geophys. Res. Solid Earth* **2020**, *125*, e2020JB020293. [CrossRef]
30. Sakellariou, D.; Tsampouraki-Kraounaki, K. Plio-Quaternary Extension and Strike-Slip Tectonics. In *Transform Plate Boundaries and Fracture Zones in the Aegean, Chapter 14*; Duarte, J.C., Ed.; Elsevier: Amsterdam, The Netherlands, 2019; pp. 339–374. ISBN 9780128120644. [CrossRef]
31. Aránguiz, R.; Esteban, M.; Takagi, H.; Mikami, T.; Takabatake, T.; Gómez, M.; González, J.; Shibayama, T.; Okuwaki, R.; Yagi, Y.; et al. The 2018 Sulawesi tsunami in Palu city as a result of several landslides and coseismic tsunamis. *Coast. Eng. J.* **2020**, *62*, 445–459. [CrossRef]
32. Omira, R.; Dogan, G.G.; Hidayat, R.; Husrin, S.; Prasetya, G.; Annunziato, A.; Proietti, C.; Probst, P.; Paparo, M.A.; Wronna, M.; et al. The September 28th, 2018, tsunami in Palu-Sulawesi, Indonesia: A post-event field survey. *Pure Appl. Geophys.* **2019**, *176*, 1379–1395. [CrossRef]
33. Papadopoulos, G.A.; Kortekaas, S. Characteristics of landslide generated tsunamis from observational data. In *Submarine Mass Movements and Their Consequences*; Locat, J., Mienert, J., Eds.; Kluwer: Dordrecht, The Netherlands, 2003; pp. 367–374.
34. Kajiura, K. The directivity of energy radiation of the tsunami generated in the vicinity of a continental shelf. *J. Oceanogr. Soc. Jpn.* **1972**, *28*, 260–277. [CrossRef]
35. Carrier, G.F. On-shelf tsunami generation and coastal propagation. In *Tsunami: Progress in Prediction, Disaster Prevention and Warning*; Tsuchiya, Y., Shuto, N., Eds.; Kluwer: Dordrecht, The Netherlands, 1995; pp. 1–20.
36. Geist, E.L. Near-Field Tsunami Edge Waves and Complex Earthquake Rupture. *Pure Appl. Geophys.* **2013**, *170*, 1475–1491. [CrossRef]
37. Lynett, P.J.; Liu, P.L.-F. A numerical study of run-up generated by three-dimensional landslides. *J. Geophys. Res.* **2005**, *10*. [CrossRef]
38. Sahal, A.; Roger, J.; Allgeyer, S.; Lemaire, B.; Hébert, H.; Schindelé, F.; Lavigne, F. The tsunami triggered by the 21 May 2003 Boumerdès-Zemmouri (Algeria) earthquake: Field investigations on the French Mediterranean coast and tsunami modelling. *Nat. Hazards Earth Syst. Sci.* **2009**, *9*, 1823–1834. [CrossRef]
39. Dogan, G.G.; Annunziato, A.; Papadopoulos, G.A.; Guler, H.G.; Yalciner, A.C.; Cakir, T.E.; Sozdinler, C.O.; Ulutas, E.; Arikawa, T.; Suzen, M.L. The 20th July 2017 Bodrum–Kos tsunami field survey. *Pure Appl. Geophys.* **2019**, *176*, 2925–2949. [CrossRef]
40. Heidarzadeh, M.; Necmioglu, O.; Ishibe, T.; Yalciner, A.C. Bodrum–Kos (Turkey-Greece) $M_w$6.6 earthquake and tsunami of 20 July 2017: A test for the Mediterranean tsunami warning system. *Geosci. Lett.* **2017**, *4*, 31. [CrossRef]
41. Amato, A. Some reflections on tsunami Early Warning Systems and their impact, with a look at the NEAMTWS. *Boll. Geofis. Teor. Appl.* **2020**, *61*, 403–420. [CrossRef]
42. Evelpidou, N.; Karkani, A.; Kampolis, I. Relative Sea Level Changes and Morphotectonic Implications Triggered by the Samos Earthquake of 30th October 2020. *J. Mar. Sci. Eng.* **2021**, *9*, 40. [CrossRef]